*Journal of Structural Geology*, Vol. 15, Nos 3–5, pp. 391 to 402, 1993
Printed in Great Britain

0191–8141/93 $06.00+0.00


# Compatibility constraints on folded and faulted strata and calculation of total displacement using computational restoration (UNFOLD program)

JEAN-PIERRE GRATIER and BERTRAND GUILLIER

L.G.I.T.-C.N.R.S., Observatoire de Grenoble, Université Joseph Fourier, I.R.I.G.M., BP 53X, 38041 Grenoble, France

(*Received* 30 *December* 1991; *accepted in revised form* 14 *September* 1992)

**Abstract**—A balanced-surface method is proposed that allows one to test the reliability of the interpretation of the structural geometry of folded and faulted strata. It also estimates both the finite total displacement field linked to the folding and faulting processes and the finite displacement field linked to the folding. The method describes a thin competent folded and faulted sedimentary layer using rigid (triangular) elements, their sizes depending on the curvature of the surface. The elements are laid flat (and are automatically fit) to form a horizontal surface, which represents the initial state of the layer. The degree of compatibility (given by different indicators) tests the reliability of the geometric fitting of the layer. If folding and faulting occur without bed stretching (or if this change is known and introduced as a parameter in the code) a plausible interpretation can be perfectly retrodeformed, just as a folded and torn sheet of paper may be smoothed with an iron. The method has been applied to two natural examples in oil-field regions using three- or two-dimensional depth-migrated seismic data. The main results reveal in general that the petroleum company's interpretations of the data were non-optimal. A careful reinterpretation of the seismic data was necessary to obtain balanced folded and faulted surfaces. The estimation of the finite displacement fields revealed the compatibility between fold and fault deformation, and also the strike-slip movement or rotation associated with the deformation.

## INTRODUCTION

IN ORDER to draw geological structures such as folds and faults, interpolation is generally needed between scattered data. Maintaining geometric compatibility between data is necessary to constrain the interpolations. To paraphrase Ramsay & Huber (1987, p. 543), "compatibility implies that the body translations, rotations and strains developed in a deformed mass obey geometric rules that are requisites for the rock mass to remain coherent after deformation". The problem is then to know how such geometric constraints may be tested. Various authors have already discussed this problem. The interpretation of continuous and discontinuous deformation is briefly reviewed below.

For continuous deformation analysis, strain–displacement relations were given in Jaeger (1956), Ramsay (1967, 1976), Howard (1968) and carefully detailed in Ramsay & Huber (1983). A major problem was the interpretation of heterogeneous deformation. A method of spatial integration of heterogeneous strain within shear zones was proposed by Ramsay & Graham (1970). In the general case, exact two-dimensional expressions for rotation gradients in terms of strain gradients were derived by Cobbold (1977). With such a continuous deformation, true strain values are necessary to obtain a unique solution for the rotations, and the accuracy of natural strain values is usually not sufficient to apply these relations.

Following another approach for the interpretation of heterogeneous deformation, Oertel (1974) has introduced the practical notion of domains (or finite elements) within each of which the strain could be assumed to be homogeneous. Schwerdtner (1977) has shown how translations and rigid rotations are necessary to ensure maximum compatibility between finite elements. This finite element method was used by Oertel & Ernst (1978) to remove the deformation in a multilayered fold, the fitting of the elements being done by hand. In order to obtain faster and more objective restoration, a least-squares method to fit the elements was proposed by Cobbold & Percevault (1983). This method was successfully applied to the removal of regional ductile strain in central Brittany (Percevault & Cobbold 1982). Application of a three-dimensional finite element method to strain field analyses (in an Archean greenstone belt) was also done by Schultz-Ela (1988). The same finite element analysis method was applied to a folded and faulted regional analysis by Gratier *et al.* (1989) with elements of about 15 × 15 km in initial size. However, in this last approach, since deformation must be assumed to be homogeneous within each finite element, the deformation values associated with faults must remain negligible compared to the deformation values associated with folds.

With continuous heterogeneous deformation, the various proposed methods are satisfactory provided that strain measurements can be collected. The major problem, of course, is that the assumption of continuous deformation ignores continuous–discontinuous partitioned deformation (such as occurs in folded and faulted structures).

With structures involving both folding and faulting, a problem occurs in considering a set of isolated data (outcrops, seismic reflectors, structures in boreholes) which yield from place to place the exact location of a

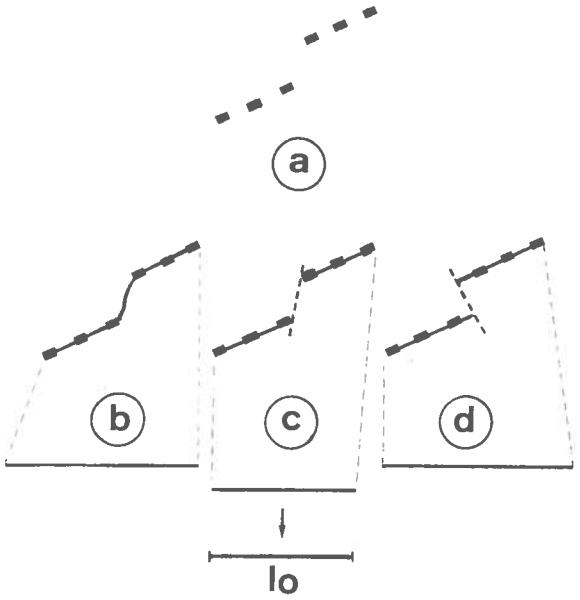


Fig. 1. For a given set of data (from seismic or geological investigations) that provides the position of a competent layer at a discrete number of points in a vertical cross-section (a), different interpolations for the geometry of the layer (thick line segments) may be done, either continuously (b) or discontinuously (c & d). In the latter case, the dip of the fault (thick dashed line) is not constrained by the available data. If the initial length of the layer ($l_o$) is known or constrained by neighbouring data, it is possible to choose among the different interpolations (here the interpretation given in c is the best: $l_o(c) = l_o$). This is the principle of the balanced cross-section construction technique, with a plane strain assumption. In order to balance a folded and faulted layer, the same approach using a trial and error method is proposed (see Fig. 2).

folded and faulted layer (Fig. 1a). There are always several possibilities of how to draw this layer (how to interpolate between the scattered data): either continuous interpolation between the data (Fig. 1b) or discontinuous interpolation (with faults). In the latter case the boundaries of the faults are generally difficult to establish (Figs. 1c or d, for example) since data are not always well-constrained near faults.

If both the initial length of the layer and the depth of the décollement surface are known, and applying the assumptions of conservation of volume, surface and length of the strata (Chamberlin 1910, Goguel 1952), it may be possible to choose between various interpolations by a trial and error method. This is the efficient principle of balanced cross-sections (Dahlstrom 1969, Hossack 1979). Several authors have developed computer programs for section balancing (e.g. Groshong & Usdansky 1986, Jones & Linsser 1986, Kligfield *et al.* 1986, Medwedeff & Suppe 1986, De Paor 1988, Moretti & Larrere 1989). Such balanced cross-section construction methods are limited, however, to two dimensions with a plane strain assumption. If this assumption is correct when the axial directions of fold hinge lines and the strike of the faults are more or less parallel, it generally becomes invalid in arcuate fold and fault zones (Ramsay & Huber 1987).

Assuming simple fault and fold kinematics, for example, if all the slip vectors for the faults (Barr 1985) or flexural-slip folds (McCoss 1988) have parallel map projections, direct three-dimensional restoration is possible. However, in this case the simplicity of the kinematics limits the application of the method.

In summary, the test of geometric compatibility of the data is, in principle, very simple (Ramsay & Huber 1987, p. 543); the geometric features of any folded and faulted stratum must be restorable to an initial undeformed state without loss of volume (or with a known volume change). With three-dimensional folded and faulted strata, the problem is then first to restore the folded zones to their undeformed state, and secondly to fit the unfolded zones along the faults. As for section balancing, this must be done by a trial and error approach which allows the integration of the entire available data. At the end of the process a balanced geometric interpretation is obtained which allows one to estimate a finite displacement field.

## PRINCIPLE OF THE METHOD

A well-drawn sedimentary layer, folded and faulted without change of thickness, and without stretching parallel to its neutral surface, can be unfolded and restored to its initial horizontal state, just as a folded and torn sheet of paper may be smoothed with an iron, where the elements are fitted without voids and overlaps. If such a fit cannot be obtained with a natural layer, this means either that the assumption of the non-elongation of the surface was not correct, or that the interpretation of the data was non-optimal. The first hypothesis may generally be tested by structural studies; if strain values are measured these values may be included in the restoration, or the choice of the layer must be limited to a folded and faulted competent layer without bed stretching.

When considering only the folded zones the validity of the constant bed-length assumption may be directly tested by the isotrend analysis proposed by Lisle (1992). Following the Gauss' Theorema Egregium the non-stretch condition for a fold is that the total curvature (equal to the product of the two principal curvatures) at any point remains invariant under isometric bending. Several authors such as Bennis *et al.* (1991), Leger *et al.* (1991) and Lisle (1992) propose the use of this method to distinguish between developable and non-developable folds. The problem, which is the same as in our approach, is that for a given data set there are two possibilities for non-developable surfaces: either bed stretching or non-optimal interpolation between the data. The application of this method to the restoration of a developable surface is also suggested by Lisle (1992), but two practical difficulties have to be overcome: "(i) the restoration by rotation has to be carried out for the whole sheet since the change of orientation of part of the sheet depends on the integrated rotation involved in other points of the sheet, and (ii) the unrolled configuration depends on the choice of the starting point for unrolling". Our approach is to unfold the sheet with a finite element method. This allows one to overcome the

first problem. Nonetheless the second problem remains, and we have to choose one fixed element.

For our approach, the test of a plausible geometric interpretation needs three successive steps.

—First, the scattered data is interpolated by partitioning the entire folded and faulted surface into folded zones described by a single-valued *XYZ* relation (one *Z* value for each *XY* pair), with a regular Cartesian *XY* grid. This allows one to describe the surface by a network of triangular elements configured in columns and rows.

—Second, each part of these folded zones is restored to a horizontal surface, by laying flat the triangles column by column. To do this a Fortran computer code was created (named UNFOLD), which runs on workstations (IBM RISQ 6000 and SUN SPARC), Gratier (1988), Gratier *et al.* (1991), Guillier (1991).

—Third, all of these unfolded zones are fitted together with minimal voids and overlaps along their edges. In our work the third step of fitting together the unfolded parts is not automatic, it is simply done by trial and error using an interactive graphics program which allows one to translate and rotate the unfolded zones.

—Finally, the comparison between the finite deformed state and the restored initial state allows one to estimate the finite displacement field associated with the folded and faulted structure.

*Interpolation*

The first step of the program is a description of the folded surface. When considering a folded and faulted layer (Fig. 2a), the program cannot unfold and restore the entire surface at the same time. A cut-out of the layer is needed in order to obtain both a regular Cartesian *XY* grid and a single *XYZ* relation within each folded block (Fig. 2b). Some types of block boundaries are obvious, such as fault boundaries (thick lines A–B and A–C in Fig. 2a). But a cut-out is also necessary from one fault tip to another, or from a fault tip to an external boundary (dashed line A–D, Fig. 2a). In such a case, the cut line may be drawn perpendicular to the contour lines of the surface in order to obtain an unfolded surface with regular boundaries. Another type of boundary is needed when the same layer exists several times on the same vertical line (e.g. the overturned limb of a fold; thrust fault). In such cases the most practical cut can be made by following the line of vertical dip of the strata (dashed line E–F, Fig. 2a). By following these rules, each folded block is then bounded by faults, vertical layers, or lines of maximum slope, and may then be digitized on a digitizing table following the contour lines on maps, or using successive cross-sections (if the boundaries of the blocks are well defined).

Interpolation is done using a cubic spline function (de Boor 1978) included in a graphics program (GREG, Guilloteau & Valiron 1986). Such interpolators have already been used for geological applications (Evans *et al.* 1985). Another method has also been proposed using a rotated cubic interpolator (McCoss 1987), which necessitates a less powerful computer. However, a cubic spline function has already been included in the graphics GREG package, and it runs rapidly enough on our workstation. The accuracy of the interpolation step is estimated by the value of an interpolation indicator, which expresses the discrepancy between the initial data and the interpolated surface (the *Z* value associated with each *XY* position of the initial data set is compared with the interpolated *Z* value at the same *XY* position). A usual range of values for this indicator is about 0.001–0.02%. These values depend both on the number of triangles and on the distribution of the initial scattered data.

*Unfolding*

Interpolation gives a regular Cartesian *XY* grid which allows one to describe the folded surface by a network of triangular finite elements parallel to this surface. The program of unfolding may then begin: each of the triangular elements is successively laid flat, column by column, to restore the initial horizontal surface of the layer.

Three types of triangle are used (Fig. 3) (Gratier *et al.* 1991).

—The first type is defined by the first triangle (hatched triangle, Fig. 3a), its location is fixed without constraints at the beginning of the process.

—The second type consists of triangles with only one neighbour (white triangles, Fig. 3a); each triangle is simply attached to its neighbour by their two common vertices.

—The third type consists of triangles with two or more neighbours (shaded triangles, Fig. 3a). This type of triangle is fitted in the triangular hole defined by its neighbours in a manner that minimizes voids and overlaps between the triangular element and the triangular hole (Fig. 3b). When the triangular hole is defined by more than three points (up to 15 vertices after the first fitting, see Fig. 3c), a mean value is calculated for each cluster of vertices in order to have three mean vertices.

Automatic fitting of plane elements has already been discussed by several authors, such as Etchecopar (1977) and Cobbold (1979). With our computer program, a simple algorithm is used to calculate the position of each triangle in order to obtain a minimum value of the sum ($D$) of the square of the distances between the three vertices of each triangle and those of the triangular hole defined by its neighbours. Fitting is obtained both by translation and rotation, The minimum value of $D$ is obtained when its partial derivatives (translation along $X$ and $Y$ and rotation) are simultaneously equal to zero. To minimize the $D$ value by translation, the two centres of gravity of the two triangles (element and hole) must coincide (Etchecopar 1977). To minimize the $D$ value by rotation, the value of the angle between the two triangles was calculated (Gratier *et al.* 1991). This relation and its associated parameters are given in the Appendix.

The code is able to treat successive columns of various length, using the two-vertices and three-vertices

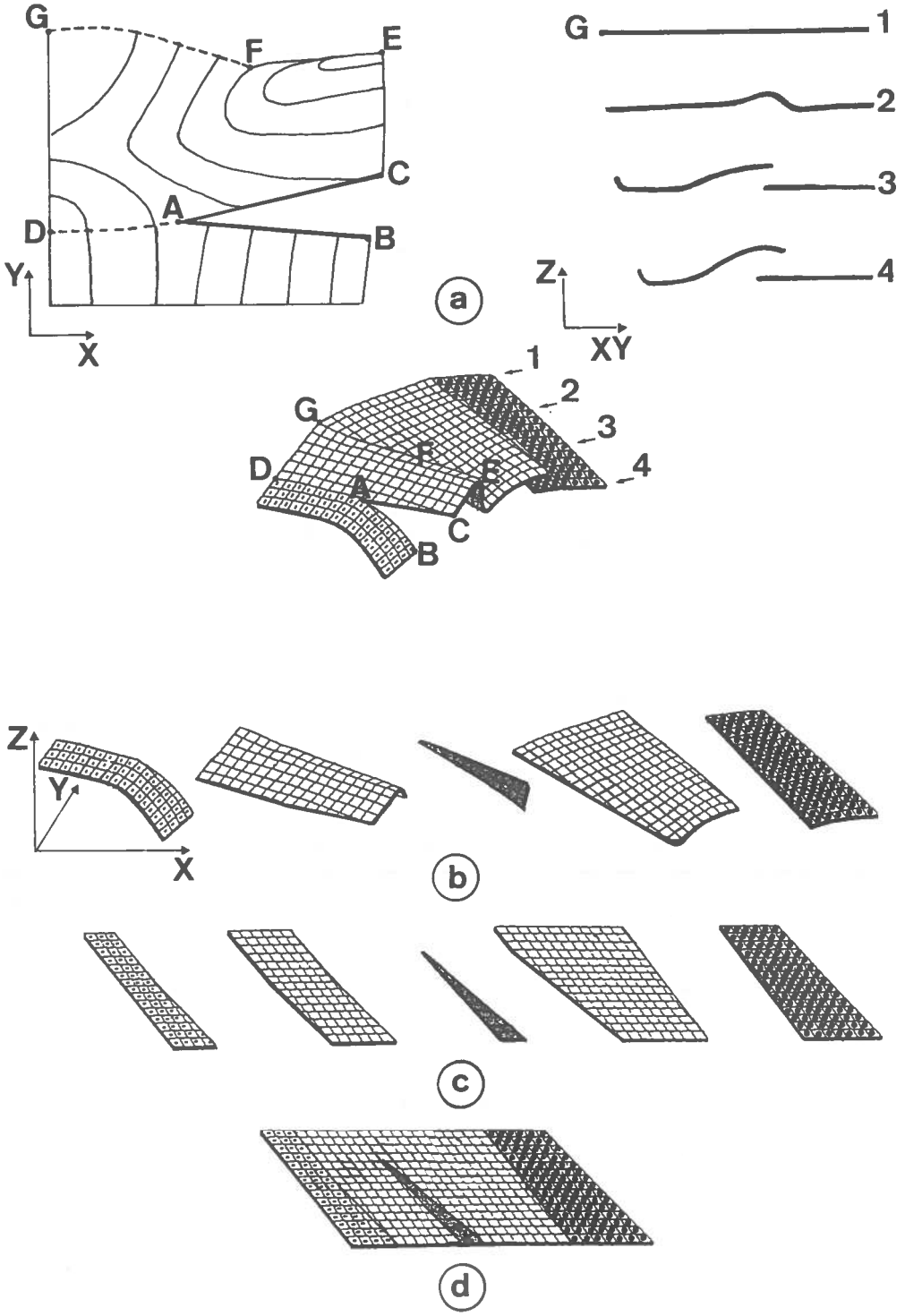


Fig. 2. Principle of the three-dimensional balance technique of a folded and faulted layer; illustrated in three successive steps. (a) The initial data set is a thin folded and faulted competent layer described by contour lines on a map (left) or by cross-sections (right). A global perspective (centre) is given in order to best visualize the data. G is a common point between the two types of representation, and the overturned limb (shaded) is not represented on the map or the cross-sections. The aim of the program is to test the geometric compatibility of this first interpretation. (b) A partition of the entire layer into folded zones with a single-valued $XYZ$ relation (one $Z$ value for each $XY$ pair) is first needed, then an interpolation is done in order to obtain a regular $XY$ Cartesian grid describing each folded zone bounded by faults (thick lines A–B, A–C in a) or by the cut out of the initial folded area (dashed lines A–D, G–F, E–F in a). (c) Each part of the folded zone is then unfolded by the computer program (UNFOLD, Fortran code running on a workstation). (d) Finally, the unfolded blocks are fitted together by a trial and error approach with an interactive graphics program on a workstation. An optimal interpretation of the data leads to an initial horizontal state without any voids and overlaps. This, of course, is possible only if the layer was deformed without elongation along its neutral surface (or with known values for this elongation, since such values may be integrated into the program).

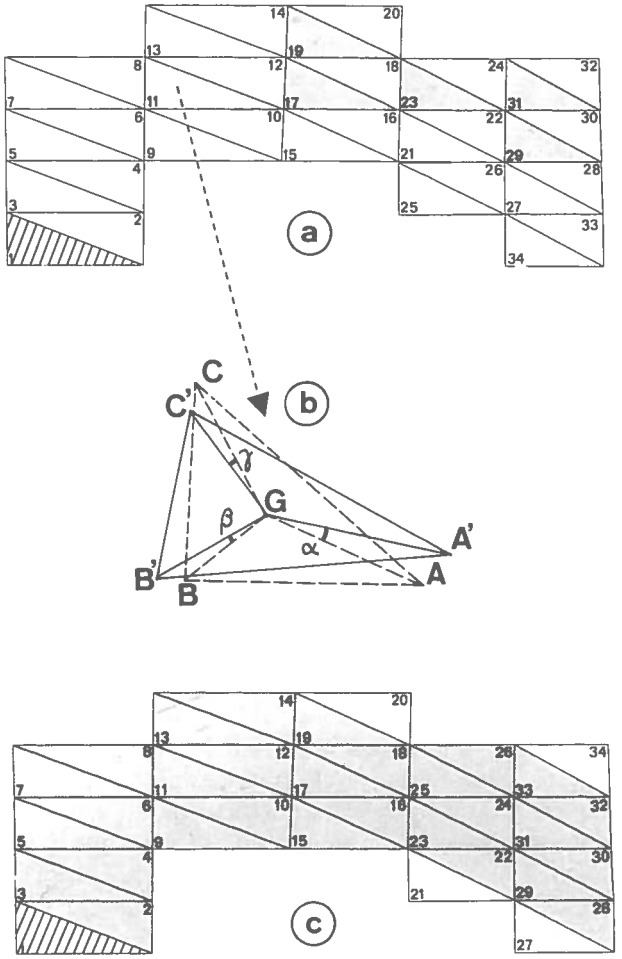


Fig. 3. After each folded surface (Fig. 2b) is segmented into triangular elements generated from points on a regular Cartesian grid, all the triangles are laid flat, column by column. (a) First fitting iteration with three types of triangles. Hatched triangle is the first triangle arbitrarily fixed. White triangles are triangles with one neighbour, attached by a common side to the preceding triangle in the laid-flat sequence. Shaded triangles are those with two or more neighbours. These triangles are fitted into a triangular hole defined by its neighbours in the laid-flat sequence. The number in each triangle indicates its rank for fitting. (b) Fitting of a triangular element ABC in a triangular hole defined by its neighbours A'B'C' (see the Appendix). For each pair of triangles (element–hole) a fitting value ($f$) is estimated as the ratio ($D/M$), $M$ being the mean value of the median length. A mean value of the fitting indicator ($F$) can also be expressed for the whole surface. (c) Successive iterations are done (i) until the mean fitting indicator value ($F$) ceases to decrease (see Fig. 4b), or (ii) until $F$ reaches a given value, or (iii) until attainment of a given number of iterations. During these iterations, most of the triangular elements are fitted into triangular holes defined by neighbour triangles (shaded), and during each iteration the new position of each triangle is used to fit the following one.

methods given above. The laid-flat succession of triangles is shown in Figs. 3(a)–(c), where the number in each triangle indicates its rank for fitting. After a first fitting of all the triangles, an approximate initial state of the layer is obtained (Fig. 3a). Several additional fittings are then done. At this stage (Fig. 3c) almost all of the triangles have more than one neighbour and the minimum distance algorithm may be used more systematically. For the second iteration, and for all of the following iterations, the position of each triangle calculated in a given iteration is used in the same iteration to calculate the position of the following triangles. This method is similar to the Gauss–Seidel method, as was pointed out by Cobbold & Percevault (1983). Each iteration calculates the distance ($D$) between the vertices of each triangle and those of its hole. For a given element–hole triangular pair, the ratio between the sum of the distance between vertices ($D$) and the mean length of the medians of the triangular element ($M$) is named the fitting indicator ($f$), and it gives the reliability of the unfolding process. This fitting indicator value can be expressed either as a mean value for the whole surface ($F$), or as local value ($f$) for each of the triangle pairs (element–hole). In the latter case a distribution map of the local value is calculated (Guillier & Gratier 1991) (see example in Fig. 4c). To end the iterative process of unfolding three types of parameter may be used: (i) the number of iterations may be fixed; (ii) the value of the mean fitting indicator, at the last iteration, may be specified (at the beginning of the process); or (iii) it is possible to let the mean fitting indicator reach its minimum value (in this case, as soon as this value begins increasing, after $n$ iterations, the process is stopped, see example Fig. 4b).

In order to estimate the usual range of fitting indicator values, various tests have been done on theoretical, experimental and natural folded structures (Guillier & Gratier 1991). The problem is to clearly distinguish between the unfolding of a developable surface and that of a non-developable surface.

(1) Developable surfaces are unfolded without any problems. An example of the unfolding of a natural layer is given in Fig. 4(a). The evolution of the $F$ value for such a surface described by 24,000 triangles (example given in Fig. 9b), is shown in Fig. 4(b). The iterative process converges relatively fast, from a mean fitting value of 3% at the first fitting to a minimum value of 0.08% after 6600 iterations. The distribution of the values of the local fitting indicator ($f$) is rather homogeneous, with values ranging from 0.76 to 0.001% (Fig. 4c). It has to be noted that, with such a developable surface, it is not worth trying to reach a minimum value for $F$. The various tests show that with a value of $F$ of about 0.2% and with a homogeneous distribution of the local fitting value (with a maximum value below 1–2%), the surface is unfolded with sufficient accuracy. Such fitting is usually obtained after some hundred iterations. In fact, as shown in Fig. 4(a), the difference between the boundaries of an unfolded developable surface after the first iteration (dashed line) and after 6600 iterations (solid line) is not very large.

The effect of direction on the successive restoration of the triangles was also tested by unfolding either parallel or perpendicular to the fold axes. For a developable surface with high dip values in the fold limbs (folded sheet of paper), there is an effect, but it is not significant with respect to the shape of the restored surface, since it remains below the approximation introduced by the segmentation of the surface into finite elements (Gratier *et al.* 1991). Therefore any side of the folded surface may be chosen as the first row to be laid flat. However, an elementary bit of caution is the avoidance of a corner

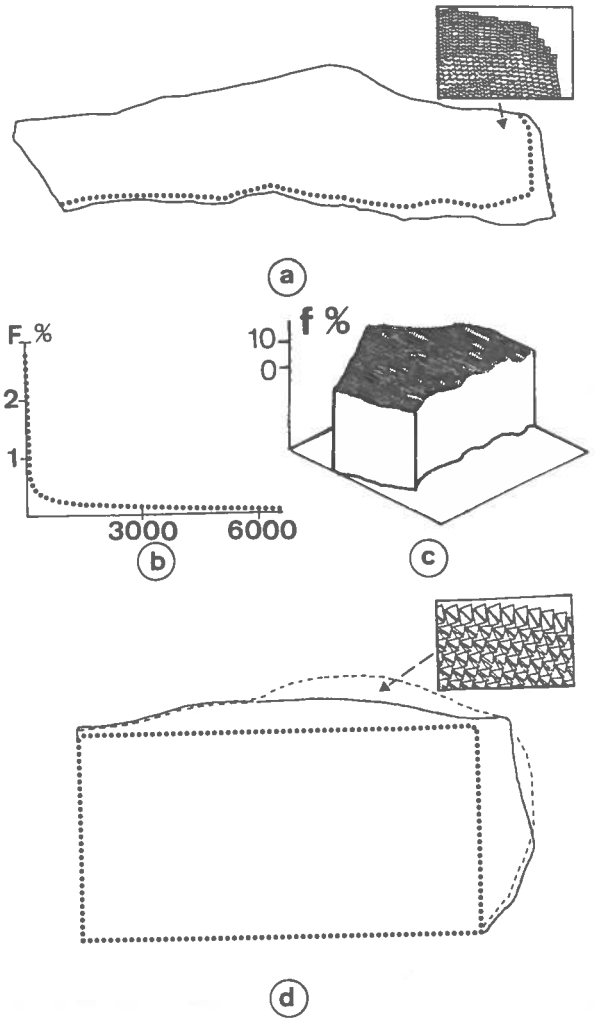


Fig. 4. Example of the unfolding of a developable natural layer (a–c) and examples of trying to unfold non-developable surfaces (d). For the unfolding of a naturally folded layer (given in Fig. 9b), the boundaries of the layer in the deformed and restored states are given in a map view (a): dotted line = deformed state, dashed line = restored state after the first iteration, solid line = restored state after 6600 iterations (the enlargement shows the triangles after the first iteration). With such a developable surface, the geometry after the first iteration is very similar to the geometry after several thousand iterations. (b) The evolution of the $F$ value vs the number of iterations ($N$) (the best fit, minimum $F$ value was obtained after 6600 iterations). (c) The distribution of the local fitting values, shown in a perspective view; these ($f$) values are relatively homogeneous between 0.76 and 0.001%. (d) Example of a non-optimal unfolding process when trying to unfold a non-developable surface (surface with small part of a dome). The boundaries of the zone are given in map view: dotted line = deformed state, dashed line = restored state after the first iteration, solid line = restored state after 600 iterations (the enlargement shows the triangles after the first iteration). With such a non-developable surface, the geometry after the first iteration is very different from the geometry after several hundred iterations. The mean fitting value, $F$, remained high (2.5%) and so did the maximum local fitting value, $f$ (20%).

with local, highly dipping strata in the first row. In some instances the first row may be imposed as a straight line.

(2) It was also interesting to test the program on a non-developable surface, such as a dome-shaped surface. Fortunately, in most cases, the program failed; the triangles could not be fitted, since after a few columns were laid flat no space was available to fit further triangular elements into the holes defined by previously processed triangles.

It may occur that a non-developable surface (a surface with only a small part of a dome) may be unfolded by the program, in which case it may then possibly be confused with a strictly developable surface. In this case, the values of the fitting indicators are very different from those of a truly developable surface. For example, in Fig. 4(d), the mean fitting indicator value reaches 2.5%, and the maximum local fitting indicator value (for the least well-fitted pair of triangles) reaches 20%. Such values clearly indicate a non-optimal unfolding run.

Another test, shown in Fig. 4(d), is the large difference between the boundaries of an unfolded, non-developable surface after the first iteration (dashed line) and after several hundred iterations (solid line). Another problem with such surfaces, which are non-developable but which can be (non-optimally) unfolded, is that the process often does not converge to a single minimum value but may show successive local minima. This indicates an instability in the process (linked to the strong heterogeneity of size of neighbouring triangles). In this case, there is an effect of the direction of unfolding, and the unfolded surface shows a strong asymmetry. Some change in the processing order of the laid-flat succession, or a large number of iterations, could perhaps reduce this asymmetry. We believe such non-developable surfaces should not be unfolded, except when the bed stretching values are known. In such a case the strain values can be used to change the shape of the triangular elements before the laying-flat process. This possibility is integrated in our program but we have never found a documented natural example to test it.

The program must only be able to recognize non-developable surfaces. As noted above the various tests have indicated that a mean fitting value of about 0.2% and a homogeneous distribution of the local fitting values (with maximum values below 1–2%) are sufficient for a surface to be unfolded. If a given natural layer is unfolded yielding higher values for the fitting indicators there are, at least, two possibilities: (i) with very well-constrained data bed stretching may be suspected; and (ii) with non-optimally constrained scattered data the structure contour map may need amending.

*Restoration*

In our approach, the third step of fitting together the unfolded blocks (Figs. 2c–d) is not automatic; it is simply done, using an interactive graphics program by trial and error. An automatic fitting program for rigid blocks has been developed by Audibert (1990) and Rouby *et al.* (in press). It may be useful as a complement to our code, but it is not absolutely necessary in a trial and error method since we will show that the major problem is related to the misinterpretation of the initial data set (see application to natural structures).

When proceeding by such a trial and error method, the various types of fold zone boundaries may be treated differently. For example (Fig. 2), the boundaries corresponding to the cut-outs of initially continuous folded zones (e.g. vertical strata and cut-outs between two fault

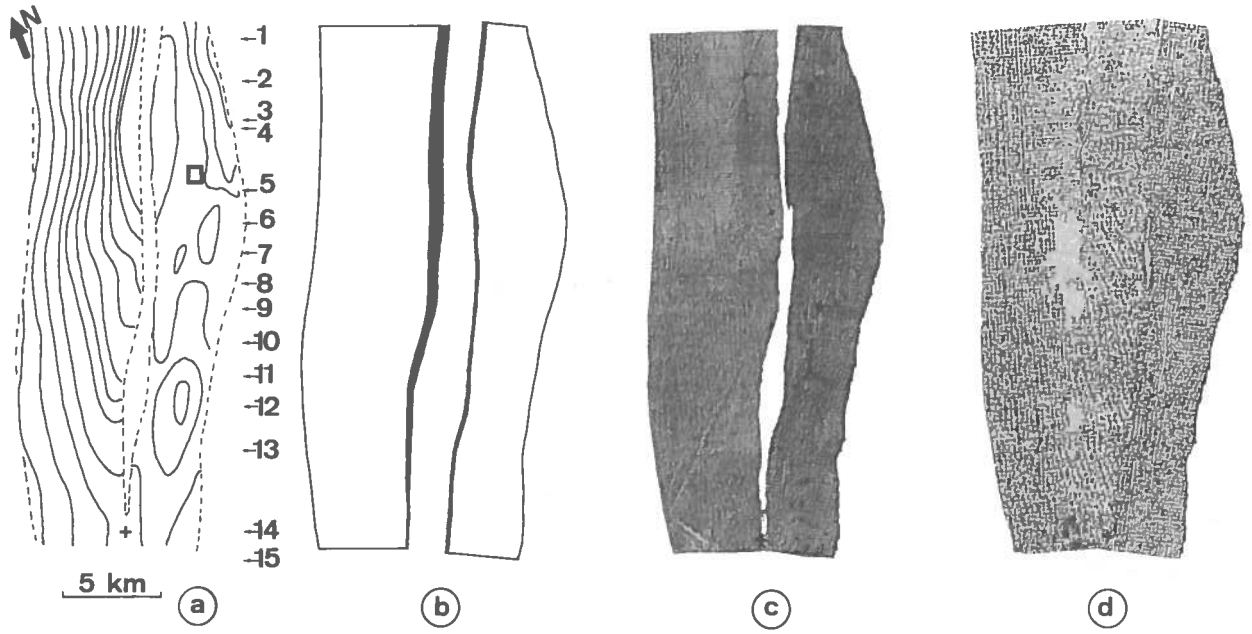


Fig. 5. First example from the continental Americas. (a) Data from successive depth-migrated seismic cross-sections were available as structure contour maps of two competent folded and faulted layers (see also Fig. 6a). The contour interval is 200 m. Only the upper layer is shown here, with a hanging-wall zone (left) and a footwall zone (right). The dashed lines indicate the boundaries of the available data; arrows with numbers indicate the locations of the seismic cross-sections. The square symbol is explained in Fig. 6. (b) Unfolding of the two zones showing the change in shape (black coloured regions) between the folded and unfolded zones (in map view). (c) First fit of the two unfolded blocks of the upper level. Large voids remain along the fault boundaries. (d) Best fit of the two unfolded blocks after reinterpretation of the initial geometry (Fig. 5a). Extrapolation of the layer is shown on the cross-sections of Fig. 6(a) (dashed lines).

tips, drawn as dashed lines) must have exactly the same length on the two parts of neighbouring zones. By contrast, the true fault boundaries (thick lines) may present some misfits if the interpretation is non-optimal. By the trial and error method successive unfoldings of the same layer (after different interpretations of the data set) may be very helpful in constraining the geometry of this layer.

## APPLICATIONS TO NATURAL STRUCTURES

We have applied our method to several naturally deformed structures from oil field areas. Two examples without locations (for proprietary reasons) are given here.

### *Area of folds and thrusts*

The first example is an oil field area in the continental Americas. Two-dimensional depth-migrated seismic data were used to define two competent layers near a thrust fault (in several dozen transverse sections and several longitudinal sections). An example of the available data is given in Fig. 5(a), which is a structure contour map of the upper level, and four cross-sections are given in Fig. 6(a). The thrust fault (sections Nos 4 and 8) fades away laterally and becomes a continuously folded surface (section No. 12) which also dies out near the southern limit (section No. 15).

The first step of the study was to insure against a non-optimal interpretation of the structures, by testing the geometric compatibility of the folded and faulted structure. The second step was to establish the finite displacement field. After making cut-outs, digitization and interpolation, four folded blocks (described by 12,000–18,000 triangles) were unfolded. Each folded zone was unfolded without a problem: minimum fitting indicator values, $F$, were obtained after about 2000–4000 iterations, and they were very low (0.025–0.05%). Also, local fitting values were homogeneous. The mean fitting values are between those obtained by unfolding a theoretical fold (0.005%) and a folded sheet of paper (0.2%). This indicates that these two competent layers are developable surfaces. If the folding process occurred without bed stretching this means that the shapes of the layers are geometrically plausible. The displacement values associated with the unfolding process show two types of change from south to north. For the upper level, the hanging-wall folded surface (left, Fig. 5b) shows an increase in displacement from south to north; in contrast, the footwall folded surface (right, Fig. 5b) shows relatively constant displacement all along its entire length. The same change was observed for the lower layer.

A major problem arose when fitting was done along the faults (Fig. 5c). This fitting was done with the following constraints: for the upper layer, two points along the thrust fault are well known. The first is an outcrop (white square Figs. 5a and 6a) located between sections 4 and 5 at the hanging-wall cut-off. The second is the termination of the folding zone (cross, at the southern part, which the two initial zones share, Figs. 5 and 6). When respecting these imposed constraints the

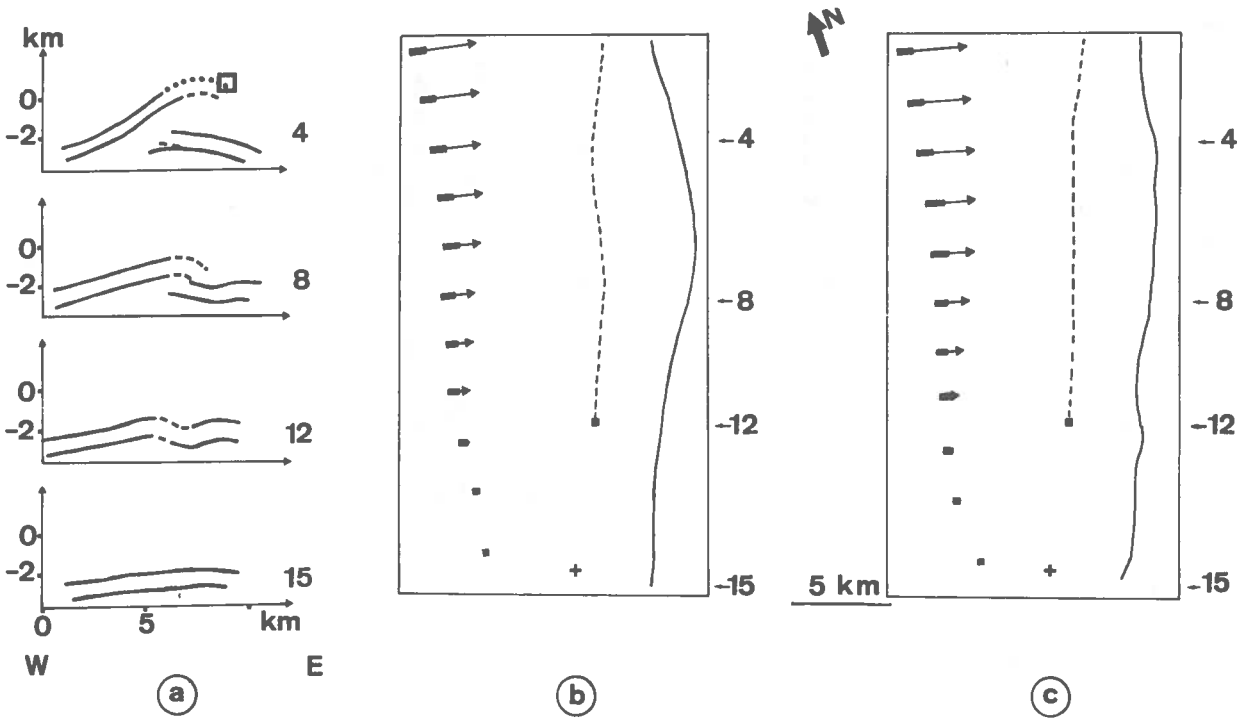


Fig. 6. Finite displacement field associated with the restoration of the first example. (a) The four cross-sections give the geometry of the two competent layers which are continuously folded in the southern part (section Nos 12) and associated with a thrust fault in the northern part (sections Nos 4 and 8). The continuous lines are the geometry as provided by the petroleum company, the dotted line is the eroded part of the upper layer, and the dashed lines are the modifications introduced by the balancing. A hanging-wall cut-off of the upper layer against the thrust fault occurs in outcrop (white square, section 4) 2500 m above the given layer (see also, Fig. 5a). (b) Finite displacement field, for the upper layer, obtained by a comparison of the present (deformed) state (Fig. 5a) and the initial (restored) state (Fig. 5d). Arrows indicate the total displacement (fault + fold) and the thick parts of the arrows indicate the displacement linked to folding. The dashed line indicates the western limits of the footwall, the black square the tip of the thrust fault, and the cross the southern termination of the fold zone which accommodates the thrusting movement laterally. (c) Finite displacement field, for the lower layer, with the same legend as (b).

fit was not good because large voids remained between the two unfolded zones. Strike-slip displacements, acting as transfer faults, could account for this misfit, but such structures do not appear on the oil company structural map. Assuming continuous thrust movement, the voids may have two explanations. (i) The part between the outcrop and the northern part of the region is simply linked to the erosion of the layer. The missing area has to be added between this outcrop and the eastern limit of the hanging-wall surface (dotted line, Fig. 6a, section 4, upper level). (ii) Alternatively, the part between the outcrop and the southern part of the region is presently underground and the misfit may result from a non-optimal interpretation of this layer.

Examination of the seismic sections supports the idea of adding area to the hanging-wall surface, but the exact eastern boundary of this folded surface does not appear clearly. To determine the length of the layer added in each cross-section, the following rules were used: (i) the eastern part of the (unfolded) footwall was considered as fixed; (ii) the southern common part (cross in Fig. 5a) was considered as the pole of rotation of the (unfolded) hanging wall; and (iii) the hanging wall was rotated in order to put the known boundary of this zone (the outcrop, see Figs. 5a and 6a) into contact with the western boundary of the (unfolded) footwall. The modifications introduced on the sections are shown in Fig. 6(a), (dashed lines). These modifications allowed us to redraw both the boundaries of the hanging wall of the thrust (sections 4 and 8, Fig. 6a) and the shape of the fold at the southern termination of the fault (section 12, Fig. 6a). A new unfolding and fitting run was tried (Fig. 5d) which gave better results than the first run (Fig. 5c). Nonetheless, very small voids and overlaps remained. Using the same value for the rotation angle (8°), the lower layer was also reinterpreted. Then it was unfolded and restored also with a satisfactory fit between the two initial zones. Of course it should be possible to redraw the two layers once more, as carefully as possible, in order to obtain the optimal representation of this oil field. Reinterpretation could include a review of the depth migration on the seismic sections. In addition, we note that the estimated volume of oil reserves is significantly increased by our interpretation.

After the balanced interpretation, the two states of the structure, before deformation (Fig. 5d) and after deformation (Fig. 5a), were matched in order to draw the finite displacements associated with the deformation. The finite displacement field (Figs. 6b & c) shows the (relative) rotation of the hanging wall vs the footwall. Comparison between the displacement associated with the fold (thick parts of the arrows, Figs. 6b & c)

and the total finite displacement (arrows, Figs. 6b & c) clearly shows that the folds and the thrust have comparable displacement fields. However, the folding process contributes only a small amount (2°) to the total rotation (8°). The geometry of the structure, with the lateral accommodation of the thrust movement by a fold, suggests that during the progressive rotation associated with the thrust development, the fold termination of the thrust may have laterally propagated along the present thrust line from the north (initial displacement) to the south (present state).

*Area of tilted-folded blocks, normal faults and strike-slip*

Another example is given, again in an oil field area, but in this case true three-dimensional depth-migrated seismic data were used to obtain the geometry of a competent layer. This structure is in an area of extension (offshore Asia). The data set also comprise a structure contour map of a reflective horizon (Fig. 7a), with fault zones coloured black. Two cross-sections give the structure according to the first petroleum company interpretation of the seismic data (Figs. 8a & b). The whole area was subdivided into 22 folded zones following the rules given earlier: the blocks are limited either by faults (thick lines, Fig. 7a) or by cut-outs of the folded zones (dashed lines, Fig. 7a).

The 22 tilted–folded zones, described by 8000–24,000 triangles, were individually unfolded without problems. The minimum values of the mean fitting indicator were obtained after about 2000–6600 iterations (see Fig. 4a), and they are very low (0.15–0.08%), ranging between those of the theoretical folded zone (0.005%) and those of the folded sheet of paper (0.2%). It should be noted that, for most of the surfaces, a low mean fitting indicator value (0.1–0.2%) was obtained after only several hundred iterations. All of these surfaces were then considered to be both geometrically plausible and deformed with little elongation.

As in the previous example a problem arose when fitting the unfolded blocks (Fig. 7b). Unlike the preceding example, however, no geometric constraint (tip point, outcrop) was available to help with the fitting. In such a case several possibilities for fitting exist, depending on the relative amounts of overlaps and voids. When random errors on the block boundaries are assumed, it seems logical to search for an equilibrium between overlaps and voids by minimizing the distance between the fitted blocks. This is the principle of automatic fitting: our automatic fitting of triangular elements and, on another scale, the automatic fitting of blocks in the program of Audibert (1990) and Rouby *et al.* (in press). With several tens of thousands of elements representing the folded surface, it is possible to search for an equilibrium between voids and overlap at the scale of the triangles during the unfolding process. But the assumption of random error, at the scale of the unfolded blocks, is only valid if an optimal drawing of the boundaries of the blocks can be assumed. When interpreting seismic data, the possibility of drawing a reflective layer of excessive length is not equal to the possibility of missing a part of the same layer (see also the first example, where a fitting without overlap is constrained by outcrop). In such a case, the first step requires careful reinterpretation of the data in order to choose a strategy for fitting, for example, choosing a first fit without overlap.

The strategy for the first fitting (Fig. 7b) in the second example was as follows. Seven seismic cross-sections were available for reinterpretation: on the line-drawings of the sections the length of the reflective layer could not be significantly reduced because all of the drawn reflectors seemed to be correctly interpreted. On the other hand, this length might be locally increased on some sections (Fig. 8d) in which the first interpretation missed a large part of the lower graben structure. In this case the reinterpretation of the data allows one to redraw the geometry of the faults and then to modify the geometry of the folded zone. Unfortunately, the small number of available sections did not permit the complete redrawing of the layer. A new fault pattern was proposed which respects the strikes of the faults in the original pattern, but introduces modifications to the fault dips, and consequently to the areas of the folded zones (Fig. 7c). It must be noted that only slight overlaps appear locally in the best first-fit sequence (Fig. 7b). This corresponds to some zones where the reinterpretation of the seismic data allowed us to decrease the length of the layer. However, in the most general case this reinterpretation led to an increase of the length of the layer (see Fig. 8).

It must also be noted that the general rule, given in the Introduction, of exact fitting for the artificial (cut-out) boundaries of the blocks and, in contrast, of allowing possible misfits for the block boundaries corresponding to faults was generally followed except for one of the artificial boundaries (in the southern part of the area). This boundary, which is the extension of a real NW–SE-trending fault, is shown as a dashed line (cut-out) in Fig. 7(a) and as a thick line (fault) in Fig. 7(c).

The resulting fault pattern given in Fig. 7(c) is then the best balance between the available data and the geometric compatibility of the folded and faulted layer. Of course there is the possibility of reinterpreting the whole structure by returning to the entire available data set for a better fit. The present state (Fig. 7c), however, of the folded and faulted layer may be considered as a balanced surface (in the same sense as a balanced line length on a cross-section, with respect to the available data).

The main aim of methods such as those applied here is to obtain the finite displacement field associated with the deformation. A finite displacement field was drawn by comparing the initial state and the restored state (the restored state is that given in Fig. 7b when voids and overlaps are removed by corrections to the geometry of the folds and faults). Displacement is estimated assuming that the upper part of the region is fixed (Fig. 7d). Of course, this is only a relative displacement since the translation and the rigid rotation of the whole area are not known. The finite displacement field presents a clear curvature in the eastern part. Finite displacement is trending NNW–SSE in the western part of the region

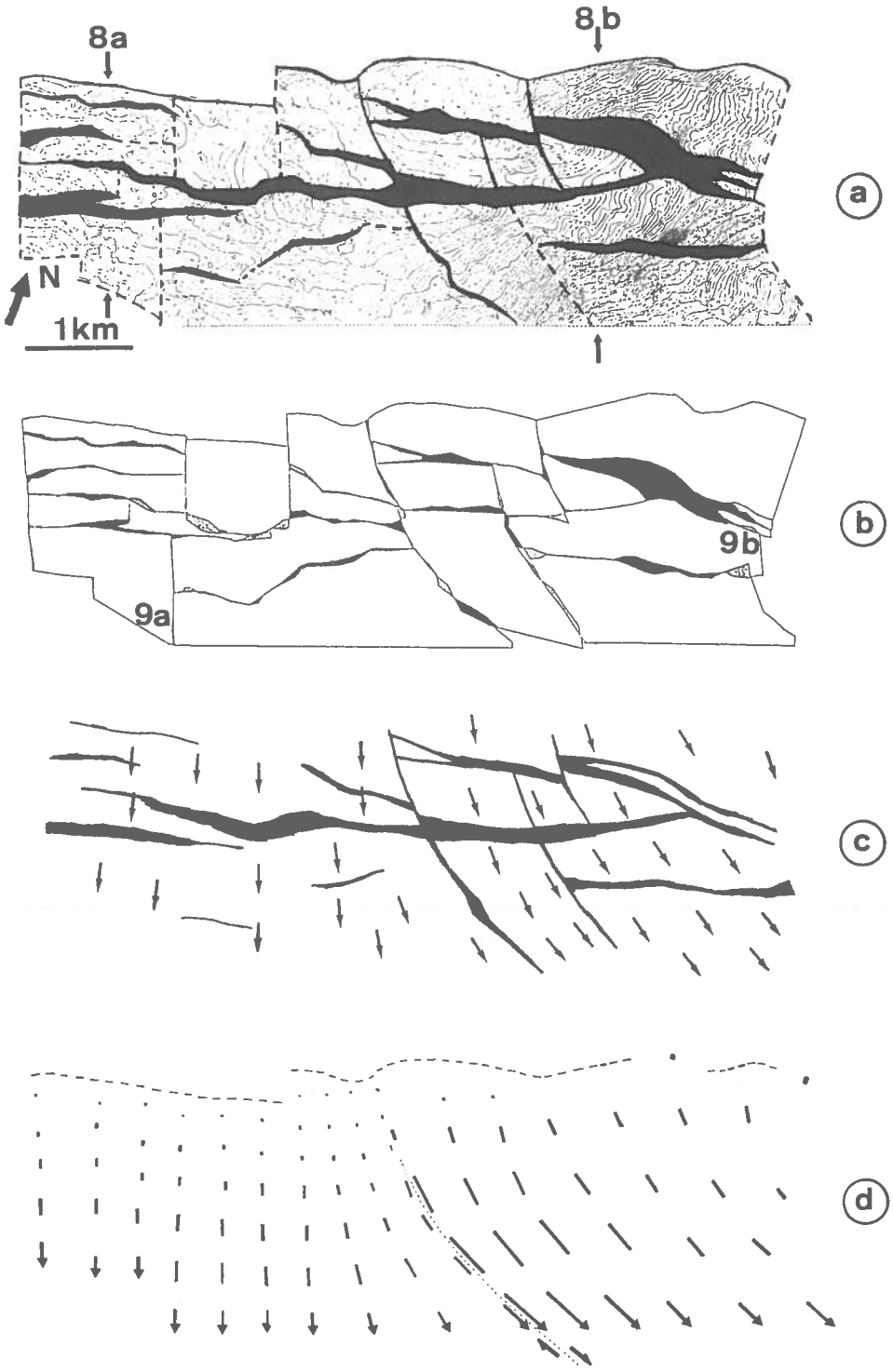


Fig. 7. Second example from offshore Asia. (a) Representation of a folded and faulted competent layer drawn from three-dimensional depth-migrated seismic data, in map view with contour lines (folded zones) and black zones (faults). The contour interval is 10 m. (b) Map-view restoration of each part of the folded layer, and first fit along the faults. The black and stippled areas represent, respectively, voids and overlaps along the fault boundaries, which may be removed by a new interpretation of the data set. A careful revision of the seismic interpretation, on seven cross-sections, indicates a non-optimal interpretation of the data (see two examples in Fig. 8), as a result of which a new fault pattern was proposed. (c) Finite displacement field linked to the unfolding, and the new fault pattern after reinterpretation of the data. Arrows indicate only the direction of unfolding. (d) Finite total displacement (from folds and faults) obtained by comparison between the present (deformed) state (a) and the initial (restored) state (b), after correction of voids and overlaps. The dashed line indicates the northern fixed boundary. The lengths of the thick lines indicate the values of finite displacement, the arrows indicate the sense of this displacement along the southern limit of the region. A clear difference appears between the eastern and the western parts of the entire region, with a curved dextral strike-slip fault (dotted line) in the median part (this fault was suggested in the first interpretation shown in a).

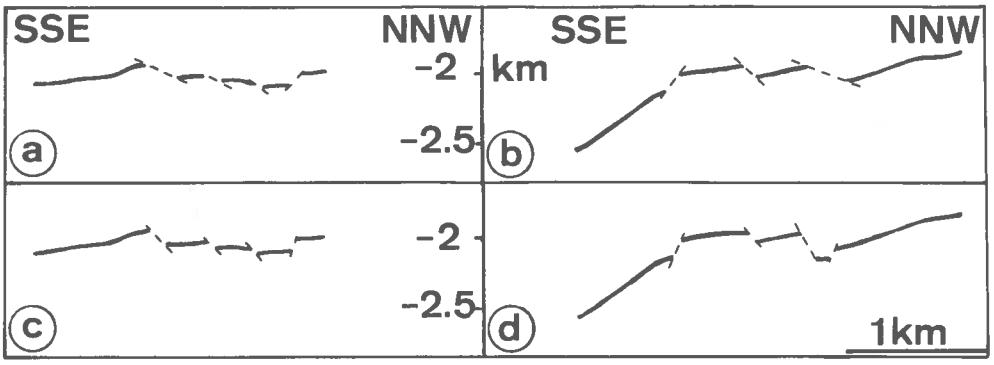


Fig. 8. Two vertical cross-sections through the structure shown in Fig. 7. (a) & (b) The geometry is as proposed by the petroleum company after the first interpretation of the three-dimensional seismic data. (c) & (d) New geometry after reinterpretation of the seismic data.

and WNW–ESE in the eastern part. If we now compare the finite displacement field (which is the sum of the displacements linked to folding and faulting) with the displacement field associated only with folding in each of the blocks (see Fig. 7c, and two examples given in Fig. 9), the two displacement fields are clearly compatible. This suggests the simultaneous development of folds (or more precisely tilting) and faults. The curved dextral strike-slip fault (given in the first structural interpretation of the oil company, Fig. 7a) is then confirmed by this restoration.

## CONCLUSIONS

After the presentation of the principles and some applications to naturally folded and faulted layers, it is useful to recall the assumptions, the limits, and the rules of the proposed balanced surface method.

—The unfolding of any layer may be done (even layers with bed stretching) providing that finite strain values are known at all points. However, since in most cases, strain values are not available, the folded and faulted layer chosen must be one in which no bed stretching occurred during the deformation (developable layer). Structural evidence may be found for a given layer to test this assumption. Most often, significant bed stretching values are associated with the development of penetrative and parallel structures (such as stylolites, solution cleavage seams and tension gashes) throughout the whole thickness of the layer. The choice of a reference layer without such structures is required.

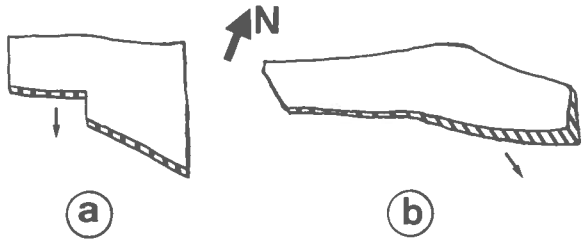


Fig. 9. Map view of the finite displacement associated with the unfolding of two zones from offshore Asia (locations given in Fig. 7). The direction of displacement (thick lines between the deformed and the restored states, see Fig. 4a) varies greatly, from a WNW–ESE displacement direction (for the east zone) to a NNW–SSE displacement direction (for the west zone).

—The test of the program on natural examples shows that such assumptions are possible for competent layers deformed under shallow crustal conditions (within the first 5–6 km of depth for competent layers such as limestones or sandstones). The natural folded zones were unfolded without problems, resulting in lower values of the fitting indicators than for the example utilizing a folded sheet of paper. This attests both to the validity of the non-elongation assumption and to the possible optimal drawing of folded surfaces using seismic data and cubic spline interpolators.

—No significant effect is associated with the direction of unfolding when unfolding a developable layer. In contrast, a strong effect of the direction of unfolding is observed when trying to unfold a non-developable layer. With such a non-developable layer the unfolding process requires the input of bed stretching values (see above).

—For the two given examples (and in other field studies which cannot be published for proprietary reasons), large misfits appear along the faults that are due to the non-optimal interpretation of seismic data near the faults. Returning to the seismic line-drawing allows one to choose the best first-fit strategy. For example, the first fit along faults may not require an equilibrium between voids and overlaps if the return to the data confirms that the voids correspond to reflective area missed during the first interpretation and if the length of the first interpreted reflector cannot be reduced. When interpreting seismic data the possibility of drawing an excess length of a reflective layer is not equal to the possibility of missing part of this same layer; it depends on the context.

—With respect to finite displacement fields, this study of natural examples shows that such displacements cannot be obtained directly from the given data, even with very sophisticated data such as three- or two-dimensional depth-migrated seismic data. It is always necessary to return to the data in order to redraw carefully the geometry of the folded and faulted surface by a trial and error method. Then, by comparison between the balanced folded and faulted layer and its restored initial state, a finite displacement field may be calculated (with an unknown bulk rotation and translation).

—For the two given examples, folding and faulting are

geometrically compatible during progressive deformation. Another constraint for such natural examples could be the use of other types of data, such as paleomagnetic measurements (for rotation–distortion), geodetic measurements, seismic focal mechanisms and striations on faults (for the displacement along the faults).

Regarding the further development of this program, two kinds of approach will be possible.

—When the décollement surface is known, a true three-dimensional balance is possible, since the transferred volume may be estimated.

—When the geometry of superimposed layers, deformed by successive steps of a progressive deformation, is available, the kinematics of the deformation can be obtained. Such examples can be found in which extension may be registered by the earliest layers and contraction by all of the layers. In this case, a step-by-step restoration of the successive events will give the step-by-step displacement field.

*Acknowledgements*—We acknowledge P. Cobbold, D. D. Schultz-Ela, R. Hellmann and A. J. Watkinson who carefully reviewed this paper, J. Letouzey who helped us with the petroleum applications, the TOTAL company who gave the data for the two examples, and the Institut Français du Pétrole for financial support.

## REFERENCES

Audibert, M. 1990. Déformation discontinue et rotations de blocs. Thèse de l'Université de Rennes. *Mém. docum. C.A.E.S.S. Rennes* **40**.

Barr, D. 1985. 3D palinspastic restoration of normal faults in the Inner Moray Firth: implication for extensional basin development. *Earth Planet. Sci. Lett.* **75**, 191–203.

Bennis, C., Vézien, J. M. & Iglesias, G. 1991. Piecewise surface flattening for non-distorted texture mapping. *Comput. Graphics* **25**, 237–246.

Chamberlin, R. T. 1910. The Appalachian folds of Central Pennsylvania. *J. Geol.* **18**, 228–251.

Cobbold, P. R. 1977. Compatibility equations and the integration of finite strain in two dimensions. *Tectonophysics* **39**, T1–T6.

Cobbold, P. R. 1979. Removal of finite deformation using strain trajectories. *J. Struct. Geol.* **1**, 67–72.

Cobbold, P. R. & Percevault, M. N. 1983. Spatial integration of strains using finite elements. *J. Struct. Geol.* **5**, 299–305.

Dahlstrom, C. D. A. 1969. Balanced cross-sections. *Can. J. Earth Sci.* **6**, 743–757.

De Boor, C. 1978. A practical guide to spline. *Appl. Math. Sci.* **27**, 57–59.

De Paor, D. G. 1988. Balanced sections in thrust belts. Part 1: Construction. *Bull. Am. Ass. Petrol. Geol.* **72**, 73–90.

Etchecopar, A. 1977. A plane kinematic model of progressive deformation in a polycrystalline aggregate. *Tectonophysics* **39**, 121–139.

Evans, D. G., Schweitzer, P. N. & Hanna, M. S. 1985. Parametric cubic splines and geologic shape description. *J. Int. Ass. math. Geol.* **17**, 611–624.

Goguel, J. 1952. *Traité de Tectonique*. Masson, Paris.

Gratier, J. P. 1988. L'équilibrage et la restauration en carte de couches plissées et faillées. In: *L'équilibrage des couches géologiques, buts, méthode et applications* (edited by Gratier, J. P.). *Mém. docum. C.A.E.S.S.* Rennes **20**, 145–157.

Gratier, J. P., Ménard, G. & Arpin, A. 1989. Strain-displacement compatibility and restoration of the Chaînes Subalpines of the Western Alps. In: *Alpine Tectonics* (edited by Coward, M. P., Dietrich, D. & Park, R. G.). *Spec. Publs geol. Soc. Lond.* **45**, 65–81.

Gratier, J. P., Guillier, B., Delorme, A. & Odonne, F. 1991. Restoration and balance of a folded and faulted surface by best-fitting of finite elements: principle and applications. *J. Struct. Geol.* **13**, 111–115.

Groshong, R. H. & Usdansky, S. I. 1986. Deformation in thrust-ramp anticlines and duplexes: implications for geometry and porosity. *Bull. Am. Ass. Petrol. Geol.* **70**, 59.

Guillier, B. 1991. Dépliage automatique de strates plissées et failléees, applications à l'équilibrage de structures naturelles. Unpublished thèse, Université de Grenoble.

Guillier, B. & Gratier, J. P. 1991. Dépliage automatique de surfaces: tests de la géométrie des strates plissées. *C.r. Acad. Sci.*, Paris **313**, 1313–1318.

Guilloteau, S. & Valiron, P. 1986. User's guide to the GREG graphic package. Observatoire de Grenoble, Université Joseph Fourier.

Hossack, J. R. 1979. The use of balanced cross-sections in the calculation of orogenic contraction, a review. *J. geol. Soc. Lond.* **136**, 705–711.

Howard, J. H. 1968. The role of displacement in analytical structural geology. *Bull. geol. Soc. Am.* **79**, 1846–1852.

Kligfield, R. Geiser, P. & Geiser, J. 1986. Construction of geologic cross-sections using microcomputer system. *Geobyte* **1**, 60–66.

Jaeger, J. C. 1956. *Elasticity, Fracture and Flow*. John Wiley, New York.

Jones, P. B. & Linnser, H. 1986. Computer synthesis of balanced structural cross-section by forward modelling. *Bull. Am. Ass. Petrol. Geol.* **70**, 605.

Leger, M., Morvan, J. M. & Rakotoarisoa, H. 1991. Inversion of 3D geological structures using parallelism, developability and smoothness least-squares criteria. In: 61*st Annual SEG Meeting*, Expanded Abstracts, 959–962.

Lisle, R. J. 1992. Constant bed-length folding: three-dimensional geometric implications. *J. Struct. Geol.* **14**, 245–252.

McCoss, A. M. 1987. Practical section drawing through layers using sequentially rotated cubic interpolators. *J. Struct. Geol.* **9**, 365–370.

McCoss, A. M. 1988. Restoration of transpression/transtension by generating the three-dimensional segmented helical loci of deformed lines across structure contour maps. *J. Struct. Geol.* **10**, 109–120.

Medwedeff, D. A. & Suppe, J. 1986. Kinematics, timing and rates of folding and faulting from syntectonic sediment geometry. *Eos* **67**, 1223.

Moretti, I. & Larrere, M. 1989. LOCACE: computer-aided construction of balanced geological cross-sections. *Geobyte* **10**, 16–24.

Oertel, G. 1974. Unfolding of an antiform by reversal of observed strains. *Bull. geol. Soc. Am.* **85**, 445–450.

Oertel, G. & Ernst, W. G. 1978. Strain and rotation in a multilayered fold. *Tectonophysics* **48**, 77–106.

Percevault, M. N. & Cobbold, P. R. 1982. Mathematical removal of regional ductile strains in Central Brittany: evidence for wrench tectonics. *Tectonophysics* **82**, 317–328.

Ramsay, J. G. 1967. *Folding and Fracturing of Rocks*. McGraw-Hill, New York.

Ramsay, J. G. 1976. Displacement and strain. *Phil. Trans. R. Soc. Lond.* **A283**, 3–25.

Ramsay, J. G. & Graham, R. H. 1970. Strain variation in shear belts. *Can. J. Earth Sci.* **7**, 786–813.

Ramsay, J. G. & Huber, M. I. 1983. *The Techniques of Modern Structural Geology, Volume* 1: *Strain Analysis*. Academic Press, London.

Ramsay, J. G. & Huber, M. I. 1987. *The Techniques of Modern Structural Geology, Volume* 2: *Folds and Fractures*. Academic Press, London.

Rouby, D., Cobbold, P. R., Szatmari, P., Demercian, S., Coelho, D. & Rici, V. A. In press. Least-squares palinspastic restoration of regions of normal faulting. Application to the Campos basin (Brasil), *Tectonophysics*.

Schultz-Ela, D. D. 1988. Application of a three-dimensional finite-element method of strain field analyses. *J. Struct. Geol.* **10**, 263–272.

Schwerdtner, W. M. 1977. Geometric interpretation of regional strain analysis. *Tectonophysics* **39**, 515–531.

## APPENDIX

The fitting of a triangular element ABC in a triangular hole defined by its neighbours A'B'C', is done as follows.

The following definitions are used (see Fig. 3): $M_a$, $M_{a'}$, $M_b$, $M_{b'}$, $M_c$, $M_{c'}$, are the lengths of the medians from G (the coincident center of mass of the triangular element and triangular hole), $\alpha$ = angle AGA', $\beta$ = angle B'GB, $\gamma$ = angle CGC'. The minimum value of $D$ (sum of the square of the distance between the vertices of the two triangles) is obtained (Gratier *et al.* 1991), when:

$$\tan \alpha = -(M_b \cdot M_{b'} \cdot \sin \beta + M_c \cdot M_{c'} \cdot \sin \gamma)/$$
$$(M_a \cdot M_{a'} + M_b \cdot M_{b'} \cdot \cos \beta + M_c \cdot M_{c'} \cdot \cos \gamma).$$

For each pair of triangles (element–hole) a fitting value ($f$) is estimated as the ratio ($D/M$), $M$ being the mean value of the median length. A mean value of the fitting indiactor ($F$) can also be expressed for the whole surface.